Supporting Information

Large-Field Electron Imaging and X-ray Elemental Mapping Unveil Morphology, Structure and Fractal Features of a Cretaceous Fossil at the Centimetre Scale

Naiara C. Oliveira[1], João H. Silva[2], Olga A. Barros[3], Allysson P. Pinheiro[4], William Santana[5], Antônio A. F. Saraiva[3], Odair P. Ferreira[6], Paulo T. C. Freire[7] & Amauri J. Paula[1]*

[1]Solid-Biological Interface Group (SolBIN), Departamento de Física, Universidade Federal do Ceará, P.O. Box 6030, 60455-900, Fortaleza–CE, Brazil

[2]Universidade Federal do Cariri, Cidade Universitária, Juazeiro do Norte–CE, Brazil

[3]Laboratory of Paleontology, Departamento de Ciências Físicas e Biológicas, Universidade Regional do Cariri, Crato–CE, Brazil

[4]Semiarid Crustaceans Laboratory, LACRUSE, Universidade Regional do Cariri, Crato–CE, Brazil

[5]Sistematic Zoology Laboratory–LSZ, Pró-Reitoria de Pesquisa e Pós–Graduação, Universidade Sagrado Coração–USC, Bauru–SP, Brazil

[6]Laboratory of Advanced-Functional Materials (LaMFA), Departamento de Física, Universidade Federal do Ceará, Fortaleza–CE, Brazil

[7]Laboratory of Raman Spectroscopy, Departamento de Física, Universidade Federal do Ceará, Fortaleza–CE, Brazil

Corresponding Author

* Tel.: +55 85 3366 9270; email: amaurijp@gmail.com

This document contains detailed information on all methods used for the large-field scanning, more specifically to obtain the electron micrographs, the X-ray elemental maps and how it was performed the dimensional analysis (for the determination of the fractal dimension of the hydroxyapatite-matrix interface). Furthermore, it contains scanning electron micrographs and X-ray energy-dispersive spectroscopy tables.

METHODS

Fossil handling

A backhoe was used to extract the fossil material during the field work. A block of shales located below the gypsum layer was removed from the Ipubi Formation. Several fossil materials were found in this block, including the shrimp species A1 studied here. The specimen was catalogued by the Laboratório de Paleontologia da Universidade Regional do Cariri (L.P.U. URCA) as Formação IPUBI no. 918. In the lab, the material was prepared using a light stereomicroscope (SMZ-1500, Nikon).

Large-Field Scanning

Images from electrons and X-rays were digitally acquired through commercial software (AZtec, Oxford). Quantification of relative concentrations by EDS (in wt%) was calculated in AZtec through a standardless method that correlates and normalises the peak intensities considering the line weight (i.e., probability of occurring each electron transition), ionisation cross-section for each element (i.e., probability of ionising the inner shell) and the X-ray absorption and fluorescence. Furthermore, the normalised relative molar concentration (NRMC, in molar units) for all elements was calculated by dividing each wt% value (provided by AZtec) by the atomic mass (g mol^{-1}) of each element, and further normalising to 1.0 the smallest relative molar concentration among all elements.

Spurious beam skirting is increased in low vacuum measurements/gas imaging. In this way, a better signal can be obtained at 20 kV due to the suppression of the beam skirting at this voltage in comparison with 5 kV. The variations in the electron and X-ray emission areas related to the interaction volume at 5 kV or 20 kV lie below the minimum spatial resolution that it was used in the determination of the fractal dimension (~25 μm). During the optimisation of the methods it was concluded that it

would be better to process the images from a minimum length scale that would not be largely affected with signal variations from the interaction volume, and the consequent electron and X-ray emission areas manifesting for regions with different chemical composition. These variations are in a scale of a few microns, considering the major elements present in the fossil: Ca, Zn, Si, S, and O. Finally, for an accurate detection and quantification of zinc, a maximisation of the ionisation cross-section for this elements is attained at an accelerating voltage slightly larger than 17 kV, at which the overvoltage (beam energy [E] divided by the ionisation critical energy [E_c]) for Zn Kα (E_c = 8.6 keV) is about 2. At the minimum length scale that was used for the dimensional analysis (~25μm), scans at pressures lower than 100 Pa provided no significant change.

Image Processing

The first step for assembling the LF images was performed in the AZtec software by combining approximately 330 adjacent images (corresponding to a sample area of 5x5 mm). The final assembly that generated the LF images was performed firstly through an algorithm (Wolfram Mathematica was used) to merge the fifteen adjacent images firstly assembled in AZtec, and then through Adobe Photoshop for repositioning the adjacent images to generate a suitable image overlapping and also for cropping unused areas. Resulting large-field images shown in the article had 5906x2119 pixels, an image definition of 600 pixel inches^{-1}, and corresponded to the whole fossil area.

A full large-field scan detecting BSE electrons takes approximately eight hours for this fossil (28 mm in length and 10 mm in width). On the other hand, the same scan detecting X-ray for rendering full elemental maps takes approximately 60 hours to perform. However, due to the sample charging, a continuous scan could be no longer

than 15 hours, and this was the reason why sample areas of just 5x5 mm were scanned in each run.

Greyscale intensity histograms in Figure 1 were obtained from images by partitioning them into boxes which quantity is defined by the number of pixels present in each image, thus resulting in one box for each pixel. Each box is labelled with a numerical value, varying from 0 to 1, which corresponds to an intensity range where zero stands for the black colour, one stands for the white colour, and values between these limits are correlated with grey tones. This numerical range is characteristic of the greyscale used for images. Therefore, greyscale images present in this article were decomposed into numerical sets (of about 1×10^8 elements) with values that range from 0 to 1, being the set size defined by the total number of pixels.

Dimensional Analysis

For the dimensional analysis, the elemental maps could provide better accuracy due to the small number of artefacts, which are practically not observed in X-ray imaging at length scales of a few tens of microns. On the other hand, backscattered electrons (BSE) emitted from the sample suffer charge interactions along the microscope chamber up to the detector, thus resulting in artefacts due to deflections and fluctuations in the signal processing. These artefacts become evident in images at the scale of tens of microns, manifesting normally as scratches and variations in the contrast function of the images. In this way, as the fossil can be revealed through its major elements, mainly phosphorus, which are not present in the matrix, elemental maps are more suitable for identifying the interface contours of the fossil. More specifically, the phosphorus map was used here because it corresponds to the hydroxyapatite phase.

The determination of white pixels corresponding to the interface of the fossil (i.e., hydroxyapatite interface) was performed by using the integral image method[1]

programmed on Wolfram Mathematica. After determining the presence of white pixels inside each box with an increasing lateral size, the fractal dimension (D, or Hausdorff dimension) was calculated from the following relation:

$$\log[N(\ell)] = A + D.\log[1/\ell] \quad (1)$$

where A is a constant, N(l) is the number of boxes with size l and l is the lateral size of the square box[2]. The precision of the algorithm used was confirmed when it was applied to fractals with known contour dimensions (or coastlines dimensions[2]), such as the Koch curve (1.2619; calculated with the algorithm: 1.2611), quadratic Koch fractal (1.5000; calculated with the algorithm: 1.4970) and Sierpinski triangle (1.5849; calculated with the algorithm: 1.5960). These deviations from the theoretical values for fractal dimensions are directly related to the image definition (i.e., pixel inches^{-1}) used in the box counting method. The minimum spatial resolution used in the dimensional analysis was ~25 μm, which corresponds to the smallest box lateral size used (5x5 pixels; one pixel corresponding to ~5 μm of the sample) in the determination of the fractal dimension of the fossil-matrix interface. This spatial resolution could be suitably attained with the image definition acquired during the individual scans (512x368 pixels; corresponding to horizontal and vertical fields of 0.41 and 0.29 mm, respectively). At this length scale, fluctuations in the contrast function originating from different ionisation volumes (after the beam interaction) and X-ray emission areas occurring for regions of the fossil with different chemical compositions can be disregarded. Possible variations in the ionisation volume and consequently in the X-ray emission areas would occur at a length scale in the order of a few microns, considering the major elements present in the fossil: Ca, Zn, Si and O[3].

The linear fit of the set of values plotted in Figure 4d alone does not represent that there is a correct determination of the dimension of the hydroxyapatite interface. Along with that, it is necessary to analyse whether the binarisation and edge-finding processes indeed produce contours that precisely correspond to the interface between the fossil and the matrix, as seen in the phosphorus map (see Figure 4a). In this way, an appropriate evaluation of binarisation and edge-finding processes must be performed in order to minimise the influence of small contrast fluctuations on how the fossil-matrix interface is defined. For this reason, the binarisation process was performed by using a small threshold value for the greyscale (i.e., 0.3) that converts darker grey tones (<0.3) to black and the rest (>0.3) to white (see Figure 4b). It was evident that the true contours of the map were not prioritised upon the fluctuations when using a threshold of 0.2 or 0.5, for instance (see Figure S1 in the Supporting Information). For more considerations regarding the dimensional analysis, see the Supporting Information.

Images used for numerical analyses (i.e. fractal dimension) have rather superior definition compared to those shown in the article: 5906x2119 pixels (600 pixel inches^{-1}), corresponding to a fossil area of 28 mm in length and 10 mm in width, with a pixel size corresponding to ~5 μm of the sample. The fossil dimensional analysis was carried out by using a box-counting approach which divides the whole image in square areas with a specific lateral size. The process is repeated 207 times in which the square lateral size was progressively increased from 5x5 pixels (smallest box size; lateral size corresponding to ~25 μm of the fossil) to 211x211 pixels (largest box size; lateral size corresponding to ~1055 μm of the fossil). Within the boxes the presence of white pixels that define the contours of the fossil was determined after the image was binarised and the contour edges rendered. The binarisation process involves the conversion of the standard greyscale that is generated by the microscope to a scale represented just by

values of 0 or 1, corresponding to black or white, respectively. After this, the edge-finding process applied a derivative function to the binarised image matrix which determines the elements of the matrix that present a non-zero derivative, thus generating the values {1,1} (white and white) for neighbouring elements {0,1} and {1,0} (black and white, white and black, respectively). For neighbouring elements of the binarised image matrix such as {0,0} or {1,1} it was generated {0,0} (black and black). Therefore any boundary present in the image is converted to a white contour. All these process were performed in Wolfram Mathematica.

After test runs it was concluded that the lowest order of the length scale could not be decreased to the nanometre scale due to large fluctuations in the contrast function at this level, because the accuracy and resolution for low vacuum analysis are lower than for high vacuum analysis. These contrast fluctuations decrease the accuracy of the dimensional analysis. As fractality is a scaling phenomenon, the highest order of the length scale could be increased to centimetres without losing the accuracy of the dimension analysis. Therefore, there is no need to decrease the lowest order of the length scale from microns to the nanometre scale.

Precisely, elemental maps and BSE images used here are in fact a projection of a three-dimensional morphology of the fossil. Images are then a construction from signals acquired along a determined thickness of the specimen that interacts with the electron beam, and this thickness is largely related with the beam accelerating voltage. Therefore, the contours and interfaces revealed in the images are projections of the fossil at a plane localised slightly below the fossil surface, more specifically localised at the maximum depth that electrons penetrates the specimen, consequently generating signal (BSE and X-rays) up to this depth. However, even considering that electrons and X-rays used for assembling the images are not rigorously emitted from the surface but

from a specific volume of the sample, the smallest length scale used for the dimensional analysis of the images was in the order of a few tens of microns (~25 μm). At this length scale it is possible to ignore possible variations in the ionisation volume and consequently in the X-ray emission areas manifesting for regions with different chemical composition. In this way, the contours and interfaces of the images are features that can be dimensionally analysed in a precise fashion, considering the existence of very small quantity of artefacts. Furthermore, it was observed in the data a perfect overlapping between the BSE and X-ray images at the length scale of a few tens of microns, which indicates that there is not a difference between the surface area of emission of electrons and X-rays at this length scale, considering the acceleration voltage (20 kV) and the beam current (~45 nA) used here. It is then possible to assume that the large-field scan with the length scales used here indeed result in reliable information on the elemental composition at a plane in the specimen, which is approximately at the specimen surface. The same would not happen if smaller length scales were used (e.g. a few microns to nanometres), because after the interaction between the electron beam and the sample, the surface area of emission of X-rays can be larger than the area of emission of backscattering electrons, because X-rays are emitted from a larger volume and deeper regions in the sample compared to BSE. In this case there would be two signals that provide morphological and compositional information of the specimen at different planes bellow the sample surface. Finally, for assuring the accuracy of the dimensional analysis, it must be also considered that the BSE T image (related to the topography) indicated that the area occupied by phosphorus is rather flat, as seen by the intensity values observed for this area (blue tones in Figure S3), which are very similar.

RESULTS

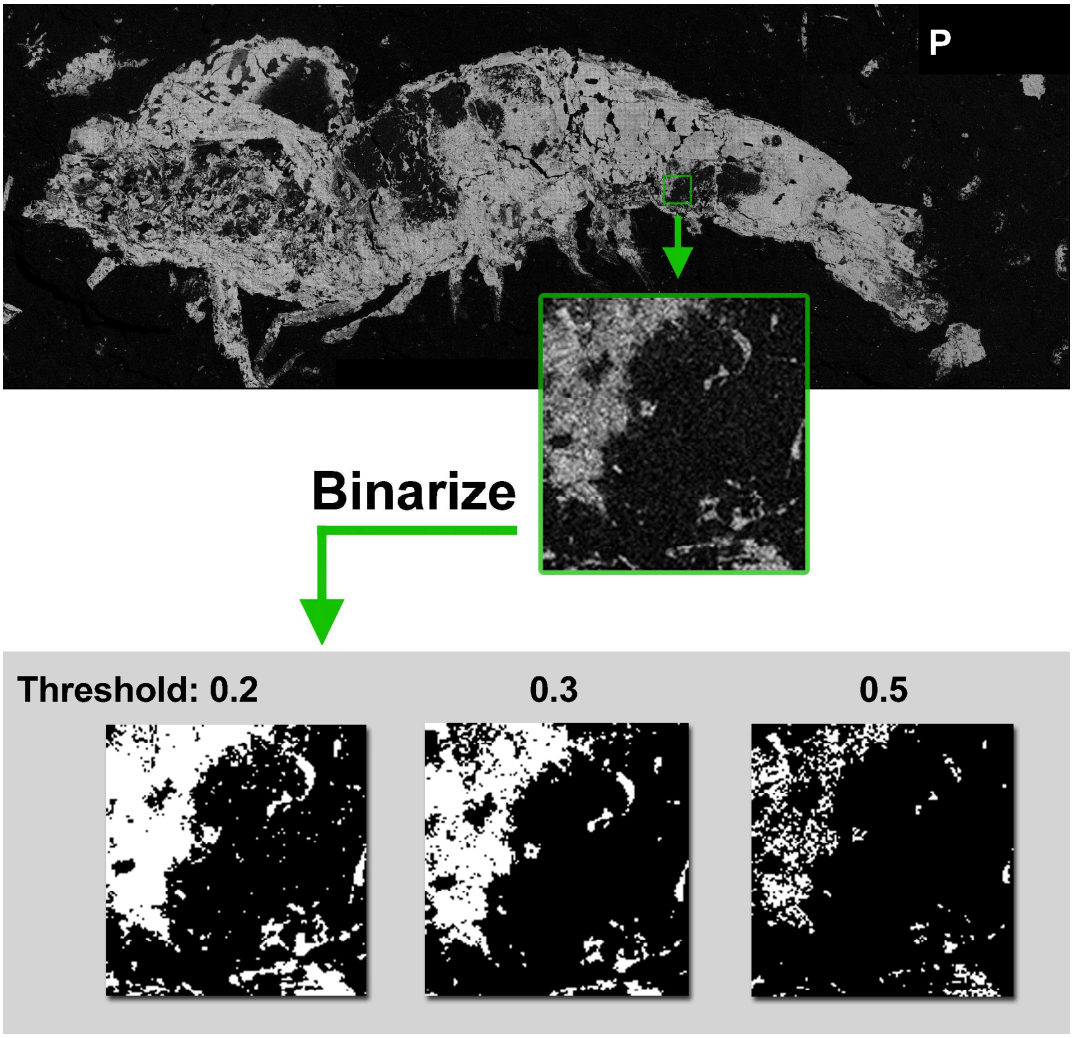

Figure S1: Result of the binarisation process for the phosphorus elemental maps using different values of threshold for the greyscale.

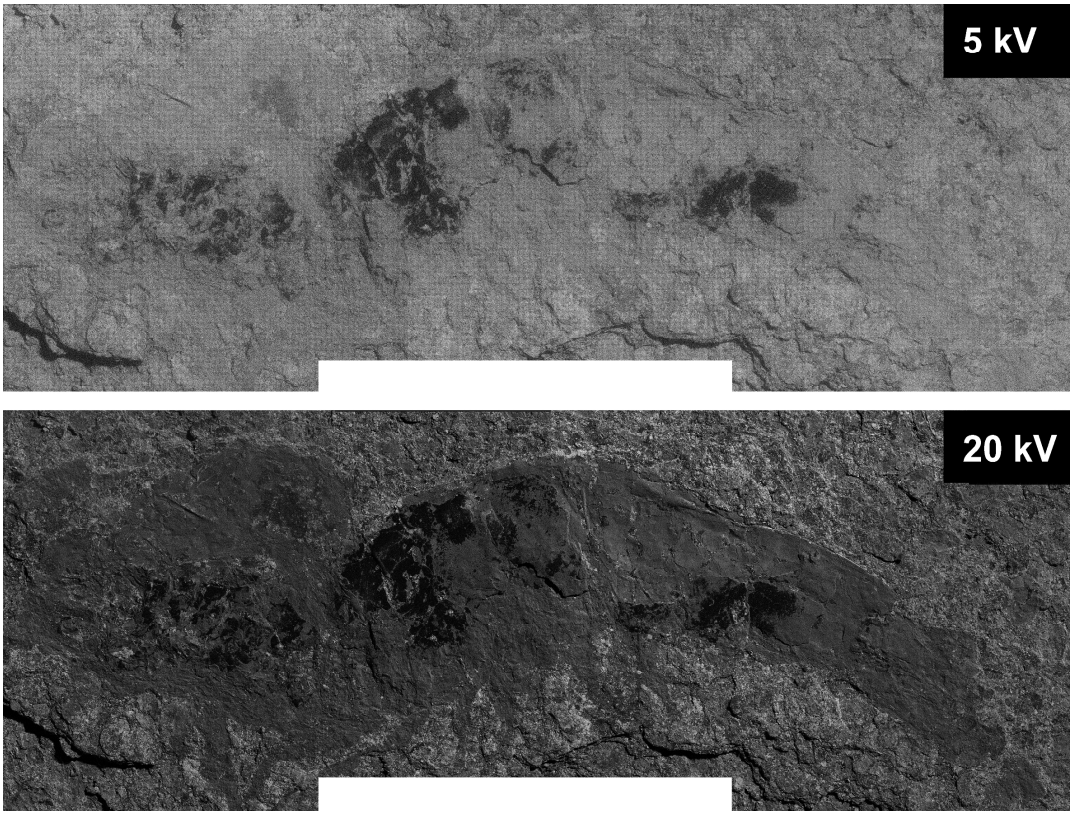

Figure S2: Comparison between oxygen (kα) elemental map obtained with the acceleration voltage of 5 kV and 20 kV. White bars stand for 10 mm.

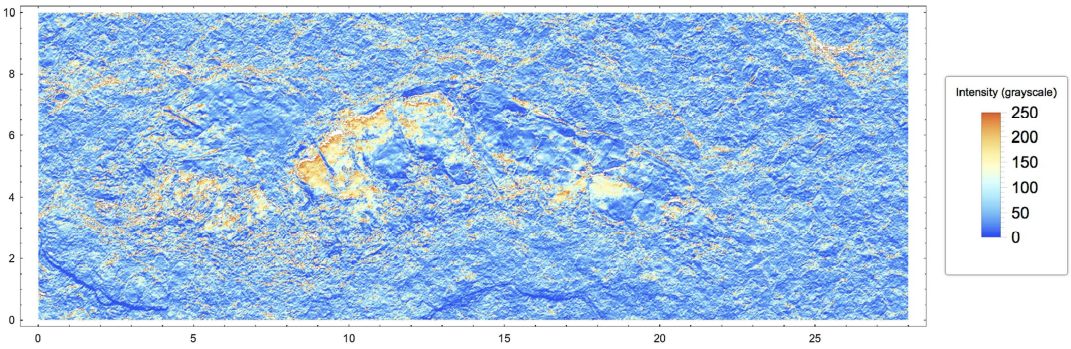

Figure S3: Density plot for the BSE T image (from Figure 1) showing the distribution of intensity values (i.e. contrast function) related to the topography of the fossil. The BSE T image analysed is in greyscale, with the intensity values ranging from 0 to 255. These values are represented here in a blue-yellow-red colour function in order to facilitate the visualization of the height differences along the image. Axes X and Y are given in millimetres (mm).

Table S1: Peak energy associated with each element identified through EDS

Element number	Element	Energy lines (keV)	Wt%
1	O	0.525	42.9
2	F	0.677	2.3
3	Mg	1.254	1.6
4	Al	1.487	3.5
5	Si	1.740	9.4
6	P	2.014	5.2
6	P	2.139	-
7	S	2.308	5.9
7	S	2.464	-
8	Cl	2.622	0.1
8	Cl	2.816	-
8	Cl	0.184	-
9	K	3.314	0.7
9	K	3.590	-
9	K	0.262	-
10	Ca	3.692	21.5
10	Ca	4.013	-
10	Ca	0.341	-
10	Ca	0.306	-
11	Fe	6.404	1.3
11	Fe	7.058	-
11	Fe	0.705	-
11	Fe	0.628	-
12	Zn	8.639	4.5
12	Zn	9.572	-
12	Zn	1.012	-
12	Zn	0.906	-
12	Zn	0.884	-
13	Na	1.041	0.6
14	Ti	4.511	0.1
14	Ti	4.932	-
14	Ti	0.452	-
14	Ti	0.401	-
15	Ce	4.840	0.1
15	Ce	5.262	-
15	Ce	5.613	-
15	Ce	4.732	-
15	Ce	6.052	-
15	Ce	6.325	-
15	Ce	4.288	-
15	Ce	0.883	-
15	Ce	1.075	-
16	Yb	7.416	0.3
16	Yb	8.402	-
16	Yb	8.759	-
16	Yb	7.580	-
16	Yb	9.780	-
16	Yb	6.546	-
16	Yb	1.521	-
16	Yb	1.765	-
16	Yb	0.190	-
16	Yb	0.179	-

Table S2: Relative quantification of the elements detected in the fossil.

Element	Atomic mass (g mol^{-1})	Cumulative: LF scan[a]		Scan at specific regions[b]					
				A		B		C	
		wt%[c]	NRMC (mol)[d]	wt%[c]	NRMC (mol)[d]	wt%[c]	NRMC (mol)[d]	wt%[c]	NRMC (mol)[d]
O	15.99	42.9	3759.3	48.9	487.9	40.3	985.2	6.5	45.4
F	18.99	2.3[e]	169.7[e]	[f]	[f]	5.6	115.3	0.2[e]	1.2[e]
Na	22.99	0.6[e]	36.6[e]	[f]	[f]	1.6[e]	27.2[e]	[f]	[f]
Mg	24.30	1.6[e]	92.3[e]	2.1[e]	13.8[e]	0.4[e]	6.4[e]	0.3[e]	1.4[e]
Al	26.98	3.5[e]	181.8[e]	5.1	30.2	0.5[e]	7.2[e]	0.6[e]	2.5[e]
Si	28.08	9.4	469.1	14.8	84.1	1.3[e]	18.1[e]	1.2[e]	4.8[e]
P	30.97	5.2	235.3	0.2[e]	1.0[e]	11.7	147.7	0.8[e]	2.9[e]
S	32.06	5.9	257.9	6.2	30.9	3.2[e]	39.0[e]	28.0	97.5
Cl	35.45	0.1[e]	4.0[e]	[f]	[f]	0.2[e]	2.2[e]	[f]	[f]
K	39.09	0.7[e]	25.1[e]	1.2[e]	4.9[e]	0.1[e]	1.0[e]	0.4[e]	1.1[e]
Ca	40.07	21.5	751.8	18.6	74.1	33.6	327.8	3.1[e]	8.6[e]
Ti	47.86	0.1[e]	2.9[e]	0.3[e]	1.0[e]	[f]	[f]	[f]	[f]
Fe	55.84	1.3[e]	32.6[e]	2.6[e]	7.4[e]	0.2[e]	1.4[e]	0.5[e]	1.0[e]
Zn	65.38	4.5	96.4	[f]	[f]	1.3[e]	7.8[e]	58.4	99.8
Ce	140.12	0.1[e]	1.0[e]	[f]	[f]	[f]	[f]	[f]	[f]
Yb	173.05	0.3[e]	2.4[e]	[f]	[f]	[f]	[f]	[f]	[f]

[a] Values calculated from the spectrum in Figure 2.

[b] Values calculated from the spectra in Figure 3.

[c] %-Weight values are relative values obtained after the calculation of the element concentration by the software (standardless method) and after the correlation and normalisation of all peaks intensities.

[d] Normalised relative molar concentrations (NRMC, in molar units) were calculated by dividing each wt% value by the atomic mass (g mol^{-1}) of each element and then by normalising the results in regard to the element present in the smallest quantity.

[e] %-Weight values for elements present in low concentrations could not be quantitatively interpreted due to the precision of the EDS method used, although they could be precisely detected.

[f] Trace elements were detected through the cumulative spectrum generated along the large-field scan, in which ~3,600 spectra were summed. These trace elements could not be detected in single spectra.

REFERENCES

(1) Viola, P.; Jones, M. *Proc. 2001 IEEE Comput. Soc. Conf. Comput. Vis. Pattern Recognition. CVPR 2001* **2001**, *1*, I511–I518.

(2) Mandelbrot, B. B. *The fractal geometry of nature*, Third.; Freeman: New York, 1983.

(3) Goldstein, J.; Newbury, D.; Joy, D.; Lyman, C.; Echlin, P.; Lifshin, E.; Sawyer, L.; Michael, J. *Scanning electron microscopy and X-ray microanalysis*, Third edit.; Springer: New York, 2003.